

ANALYZING THE IMPACT OF CLIMATE CHANGE ON NATURAL VEGETATION GREENNESS USING IMPROVED STATISTICAL VEGETATION INDEX SIMULATION MODEL

TONG, R.Z.^{1,2} – SONG, H.³ – SUN, W.C.^{1,2*} – XU, Z.X.^{1,2} – YAO, X.L.^{1,2} – YU, J.S.^{1,2}

¹*College of Water Sciences, Beijing Normal University
Xinjiekouwai Street 19, Beijing 100875, China
(phone: + 86-10-5880-2736)*

²*Beijing Key Laboratory of Urban Hydrological Cycle and Sponge City Technology
Xinjiekouwai Street 19, Beijing 100875, China
(phone: +86-10-5880-1136)*

³*Zouping Bureau, Yellow River Conservancy Commission of the Ministry of Water Resources
No. 33 Huangshan Road, Zouping, Binzhou 256200, China
(phone: +86-54-3330-7114)*

**Corresponding author
e-mail: sunny@bnu.edu.cn*

(Received 20th Dec 2018; accepted 20th Feb 2019)

Abstract. In arid regions, vegetation growth relies on water availability. Climate change can alter water cycling with subsequent effects on vegetation growth. This study examined the effects of projected climate change on vegetation greenness in the middle-reaches region of the Heihe River Basin, the second largest inland basin in China. The relationship between the Normalized Difference Vegetation Index (NDVI), an indicator of vegetation greenness derived from remote sensing data, and meteorological factors of precipitation and temperature was simulated using a modified statistical vegetation index simulation model. The model predicted that along with increases in precipitation and temperature, spring and autumn NDVI will rise about 3.8% and 7.9% by the 2050s, respectively. NDVI in summer increases about 3.9%, as increased precipitation may be superior to higher rates of soil water evaporation due to rising temperature. Hydrological processes in the Heihe River Basin are highly influenced by both climate change and human activities. The findings of this study are valuable for the development of water resource management policies that balance the water demands of both human society and the natural ecosystem.

Keywords: *NDVI, remote sensing, arid region, vegetation greenness, climate change*

Introduction

Drylands occupy more than 40% of terrestrial Earth (Slaymaker et al., 1998). The land area desertified or prone to desertification has been estimated as 57–65% of the total area of dryland ecosystems (UNEP, 1992). Land degradation in drylands has negative influences on global food security (MEA, 2005; Tschardt et al., 2012; Weston et al., 2015). Natural vegetation plays an important role in maintaining dryland ecosystem functions (Lal, 2004; Zethof et al., 2019). As a result of the tight coupling among water, energy and biogeochemical cycles in drylands, vegetation dynamics strongly influences water cycling and responses to climate change and human activity in these systems (Wang et al., 2012; Ott et al., 2016). Natural vegetation in arid regions is particularly affected by temperature and precipitation at different temporal and spatial scales (Stellmes et al., 2010; Gessner et al., 2013; Li et al., 2015). Better understanding

of plant growth responses to climatic changes will provide important insight into hydrological processes in drylands because plant growth relies on water availability.

Determination of the influence of climate change on vegetation requires long-term observation. Field observations of vegetation growth, however, are time- and labor-consuming. Remote sensing is an effective alternative way to monitor temporal trends in vegetation growth and changes in ecosystem function (Pouliot et al., 2009; Li et al., 2013; Wu et al., 2014; Liu et al., 2016). Among numerous vegetation indexes derived from remote sensing, the Normalized Difference Vegetation Index (NDVI) is widely regarded as a good proxy for terrestrial vegetation growth. NDVI, the ratio of the difference in near-infrared and red reflectance and the sum of these two variables, estimates the photosynthetically active radiation absorbed by photosynthesizing tissue (Fensholt et al., 2004). Trend analysis of NDVI data has generally been used to detect changes in vegetation dynamics at continental or regional scales. Many studies (e.g., Piao et al., 2006; Fensholt et al., 2012; Krishnaswamy et al., 2014; Wu et al., 2014) have reported strong correlations between NDVI and meteorological factors including temperature and precipitation. Los et al. (2006) built a statistical vegetation index simulation (SVIS) model to estimate the coupling strength of NDVI with temperature and precipitation using a satellite-derived monthly vegetation index and meteorological data. The model is potentially useful for predicting the response of natural vegetation to climate change in regions where field data are sparse.

The Heihe River Basin in arid northwest China is the second largest inland basin in China. The basin is adjacent to the north edge of the Qinghai-Tibetan Plateau and is characterized by diverse geomorphology. As the transition zone between the upper-reaches region of the Heihe River Basin in the southern Qilian Mountains and the lower-reach region in the northern Alxa Desert, the middle-reaches region is ecologically unique (Lu et al., 2003). It is well known for its irrigated agriculture using river water and pumped groundwater, which alters natural water cycling. Thus, natural vegetation in this region is vulnerable to both climate change and human activities (Qi and Luo, 2007; Sun et al., 2015). The objective of this study is to explore how the greenness of the *Salsola passerina*, which is an annual C4 plant and one representative plant in the middle-reaches region, responds to future climate changes by using a modified version of the SVIS model forced with a future climate change scenario. The prediction made by the model is important to develop water resource management policies that balance the water demand of human society and the natural ecosystem. A high-resolution meteorological forcing dataset was used as model input to account for the high spatial heterogeneity in dryland precipitation and temperature. The future climate change scenario was built by using the downscaled ensemble output of 16 general circulation models (GCMs).

Materials and methods

Study area

The Heihe River Basin (*Fig. 1*) originates in the Qilian Mountains in the northern edge of the Qinghai-Tibetan Plateau, covering an area of about 142,900 km². The elevation of the basin gradually decreases from the high mountain area in the south to the northern high-plain area. The Heihe River Basin is not influenced by the East Asian monsoon and has a very dry climate, with an average annual precipitation of 100–450 mm. Differences in geomorphology divide the basin into three regions: the upper-

reaches region is in the Qilian Mountains; the middle-reaches region is part of the Hexi Corridor Plain; and the lower-reaches region is on the Alxa Plateau. The middle-reaches region is the most populated. River water and pumped groundwater are the main water resources for irrigation and domestic use. Gobi and cropland are the dominant types of land cover. Cropland is mainly distributed in the oases near the main stream, and Gobi mainly occurs between the northern edge of the Qilian Mountains and the river. The *Salsola passerina* is one representative natural plant in the Gobi region.

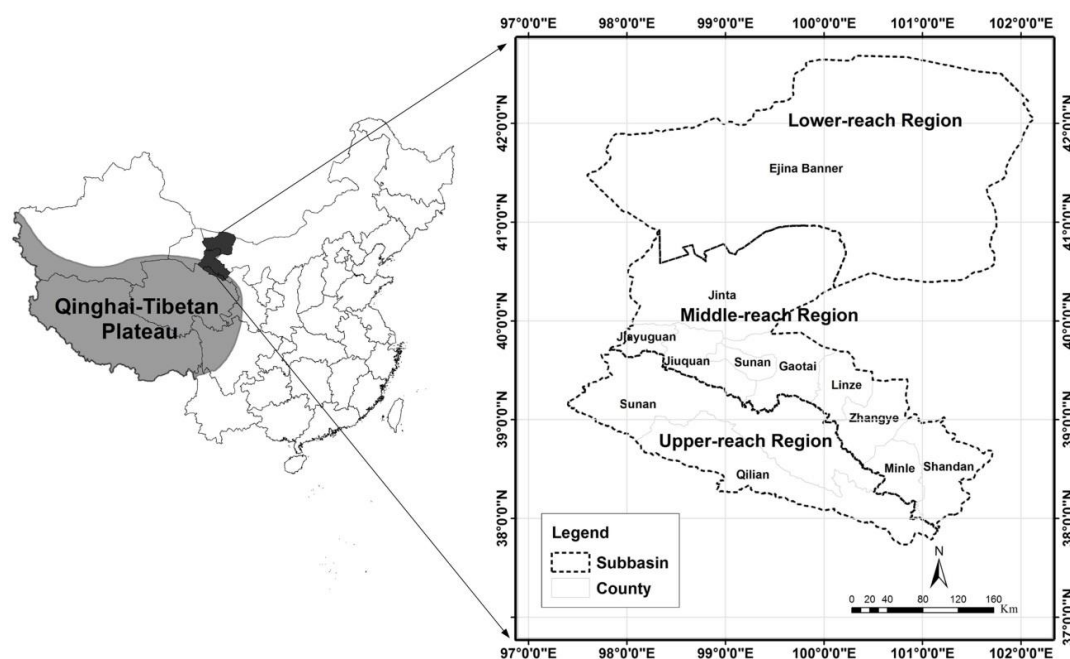


Figure 1. Heihe River Basin and its location in China

Dataset and preprocessing

The third generation of Global Inventory Modeling and Mapping Studies (GIMMS) NDVI dataset used in the study extends from 1982 to 2010 with an 8-km resolution and was obtained from NASA Ames Ecological Forecasting Laboratory (<http://ecocast.arc.nasa.gov/data/pub/gimms/>). The GIMMS data are derived from imagery taken from National Oceanic and Atmospheric Administration (NOAA, USA) satellites. Based on a field survey in 2014, a pixel of the NDVI dataset in which *Salsola passerina* was the dominant vegetation was selected for simulation. The location of the pixel and the characteristic landscape in this area are shown in *Figures 2 and 3*, respectively. To reduce the noise in the data, the maximum value composite method was used to generate 8-km resolution monthly NDVI data from the two images of each month. The averages of monthly NDVI and its standard deviation for 1982–2010 are shown in *Figure 4*. A sharp increment is found between March and April. And the NDVI in November is much lower than that in October. Following the definitions of Piao et al. (2011), NDVI averages from April to October represented the annual growing season, while April and May were considered spring, June to August were considered summer and September and October were considered as autumn. *Figure 5* shows the time series of growing season NDVI for the period of 1982–2010. No statistical trend has been detected at temporal domain.

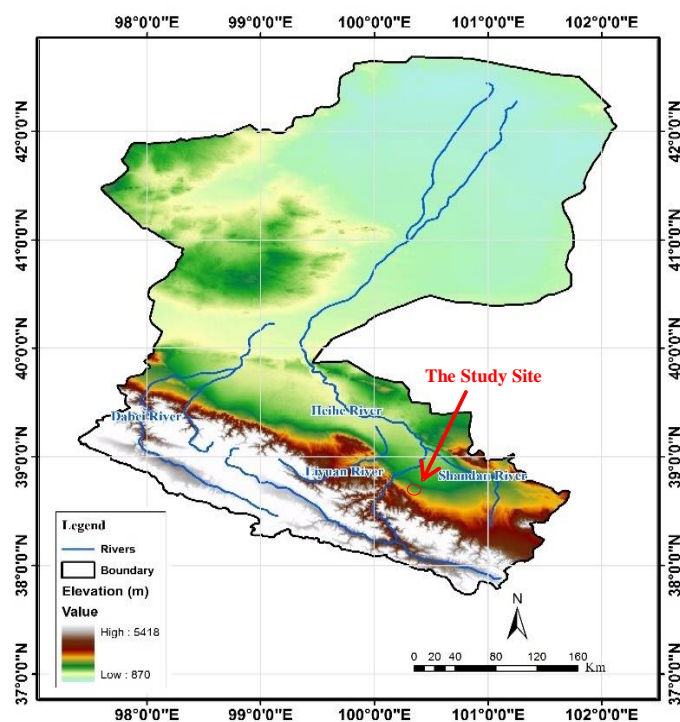


Figure 2. Location of the study site in the Heihe Basin



Figure 3. Landscape at the study site during a field survey in June 2014

The meteorological dataset used in the study covers 53 years (1958 to 2010) with spatial and temporal resolutions of 5 km and 3 h, respectively, and was developed by the Land-Atmosphere Interaction Research Group at Beijing Normal University (<http://globalchange.bnu.edu.cn/research/forcing>). Seven meteorological variables (i.e., air temperature, air pressure, relative humidity, wind speed, precipitation, shortwave radiation and longwave radiation) were produced by combining gauge observations with reanalysis data or remote sensing data (Li et al., 2014; Huang et al., 2014). The air temperature and precipitation data from the above mentioned meteorological dataset are

used in this study. Within the spatial extent of the selected NDVI pixel, air temperature and precipitation data for 1982 to 2010 were resampled to produce corresponding meteorological data. The monthly total precipitation and mean air temperature were given as the respective sum and average of the data within each month.

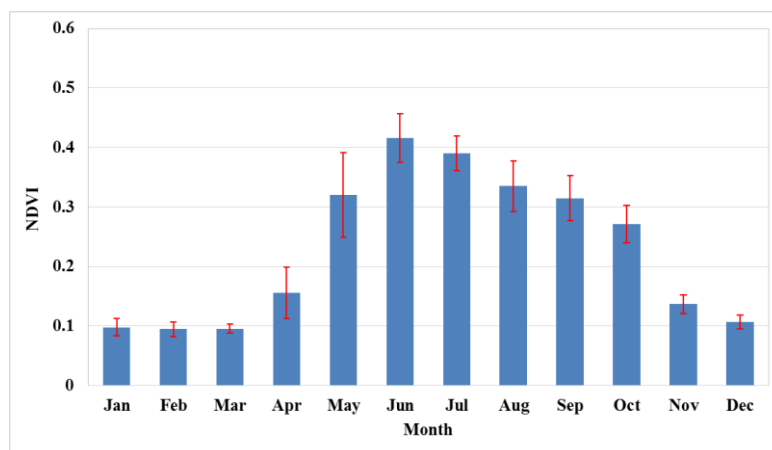


Figure 4. Mean monthly NDVI (blue bars) and its standard deviation (red lines) at the study site for 1982–2010

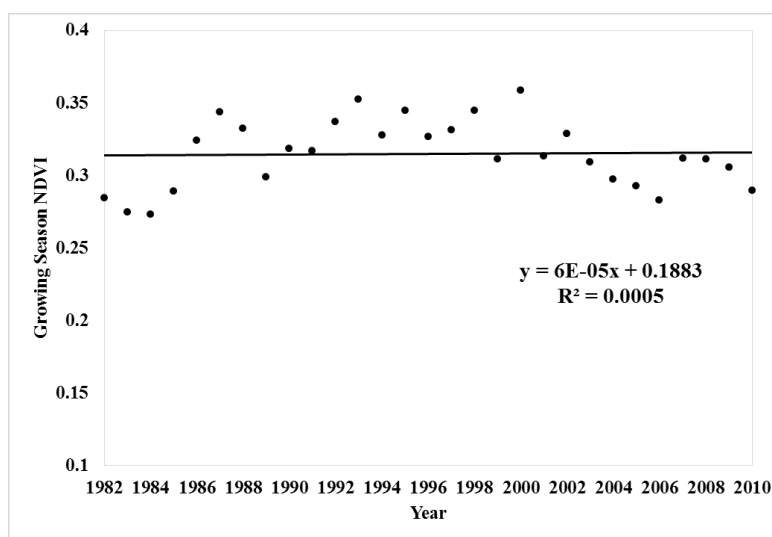


Figure 5. Time series of growing season NDVI (black dots) and its trend line (black line) for 1982–2010

Statistical vegetation index simulation model

The SVIS model is a conceptual model that investigates the relationship between vegetation greenness derived from remote sensing data (NDVI) and meteorological variables using multiple linear regression analysis. SVIS can predict monthly NDVI using precipitation and temperature data from the current month and the two previous months to account for the time-lag effect of meteorological factors on vegetation growth. The feasibility of the model was verified by Los et al. (2006). The model is defined as *Equation 1*:

$$V_t = a + \sum_{i=-2}^0 b_{t,2+i} P_{t+i} + \sum_{i=-2}^0 c_{t,2+i} T_{t+i} + \sum_{m=-2}^{-1} d_{t,2+m} V_{t+m} \quad (\text{Eq.1})$$

where P and T are the precipitation and temperature of the current month (t) and two previous months ($t-2$) and ($t-1$); V_t , V_{t-1} and V_{t-2} , are the NDVI of the current month t and two previous months ($t-2$) and ($t-1$); and a , b , c and d are parameters describing relationship between NDVI and the two meteorological variables.

In this study, rather than using multiple linear regression analysis, an Artificial Neural Network (ANN) was used to describe the relationship between NDVI and the meteorological variables. The development of ANN was inspired by the functionality of biological neural networks such as the human brain. Biological neural networks learn quickly from experiences and interactions between the internal and external environment to establish pattern recognition. ANN is recursive and can continually learn from the given dataset, which has proven to be efficient and time saving. ANN can also be used for the simulation of complex and nonlinear processes. The ANN model used in this study is of the form (Eq. 2):

$$V_i = f(P_i, P_{i-1}, P_{i-2}, T_i, T_{i-1}, T_{i-2}) \quad (\text{Eq.2})$$

where V_i , P_i and T_i are the NDVI, precipitation, and temperature of the i th month in a year; and P_{i-1} , P_{i-2} , T_{i-1} and T_{i-2} are the precipitation and temperature of two previous months ($t-1$) and ($t-2$), respectively. f represents the nonlinear relationship between the meteorological input and NDVI output derived from the ANN. The model performance indicators were the squared correlation coefficient (R^2) and the mean absolute difference (MAD) as Equations 3–4:

$$R^2 = \frac{\left[\sum_{i=1}^n (V_{obs,i} - V_{obs,a})(V_{sim,i} - V_{sim,a}) \right]^2}{\sum_{i=1}^n (V_{obs,i} - V_{obs,a})^2 \sum_{i=1}^n (V_{sim,i} - V_{sim,a})^2} \quad (\text{Eq.3})$$

$$MAD = \frac{1}{n} \sum_{i=1}^n |V_{obs,i} - V_{sim,i}| \quad (\text{Eq.4})$$

where $V_{obs,i}$ and $V_{sim,i}$ are the observed (GIMMS dataset) and simulated NDVI at time step i , and $V_{obs,a}$ and $V_{sim,a}$ are the average observed and simulated NDVI over the whole training or validation period. The simulation is made for the period of 1982 to 2010. In order to make the training period cover various climatic condition of the study site, the data of even-numbered years in this period were used to train the model. And data of odd-numbered years were used for model validation.

Future scenarios under climate change

After development, the model was applied to predict vegetation greenness under future climate change scenarios. The GCMs need to be downscaled because their outputs are too coarse to describe climatic characteristics at the regional scale. Moreover, uncertainties in climate projections from GCMs require consideration. To make a more reliable future regional climate change scenario, usually an ensemble

analysis combining multiple GCM analysis and quantifying the probability of future climate is conducted. The Climate Wizard dataset (available at: <http://www.climatewizard.org/index.html>), projections of future temperature and precipitation derived from ensemble average of 16 Coupled Model Intercomparison Project phase 3 (CMIP3) GCMs, is adopted in this study to reduce possible uncertainties of GCMs. The monthly precipitation and mean temperature was downscaled to the resolution of 50 km using an empirical statistical method (details are available in Palmer et al., 2004). The data of the 2050s (2040–2069) for A1B scenario (medium CO₂ emission) were used to build regional climate change scenario of the mid-21st century at the study site. According to the intergovernmental panel on climate change special report on emission scenario, the A1B scenario corresponds to rapid growths in economy and global population, which reaches peaks in the mid-21st century and declines following a slowing growth, and is a moderate scenario for greenhouse gas emission. This study focus on how the vegetation growth responses to intermediate climate change scenario and discussions about extreme scenario are out the scope of this study. Therefore, the climate projection under A1B scenario is used in our research. It is widely used for examining potential vegetation response in the future to climate changes in previous studies (e.g., Alo and Wang, 2008; Smith et al., 2011; Waha et al., 2013). Percentage change in monthly precipitation between projections for the 2050s and the past 50 years was used to scale monthly precipitation data for 1982–2010. The absolute difference in monthly temperature between the projected (2050s) and historical (past 50 years) climate was added directly to monthly temperature data for 1982–2010. Using the future climate change scenario as input, the NDVI prediction made by the ANN model represents the status of vegetation growth in the 2050s. NDVI simulated using meteorological data from 1982–2010 was considered the baseline. The differences between the two simulations are considered as the impact of climate change on vegetation growth. Model prediction excluded the winter period and was conducted only for months during the growing season (April to October).

Results and discussion

Seasonal fluctuation in vegetation greenness and meteorological factors

Time series of monthly precipitation, temperature, and NDVI in the Heihe River Basin from 1982 to 2010 revealed unimodal seasonal patterns (*Figures 6 and 7*). Intra-annual variation patterns in the two meteorological variables were consistent with that of NDVI. All three variables showed periodic variation with maximum values in summer or fall and minimum values in winter. Average summertime NDVI was 0.38. Average wintertime NDVI was 0.11, indicating the existence of a winter dormant period. Analysis of the multi-year averaged NDVI data from 1982 to 2010 indicated that from the beginning of spring (April) to the beginning of summer (June), NDVI increases with an average magnitude of 0.32 (*Table 1*). NDVI remained high during the two subsequent summer months. *Table 1* also shows that NDVI decreases with an average magnitude of 0.20 from the end of summer (August) to the beginning of winter (November).

For both temperature and precipitation, absolute values of the increases from the beginning of spring to the beginning of summer were smaller than that for the decrease from the end of summer to the beginning of winter (*Table 1*). In contrast, the magnitude of increase in NDVI was greater than the magnitude of decrease in the same periods,

indicating a time lag in NDVI response to changes in precipitation and temperature. This time lag was the justification for the use of both the current and the previous two months' meteorological data for monthly simulation of NDVI.

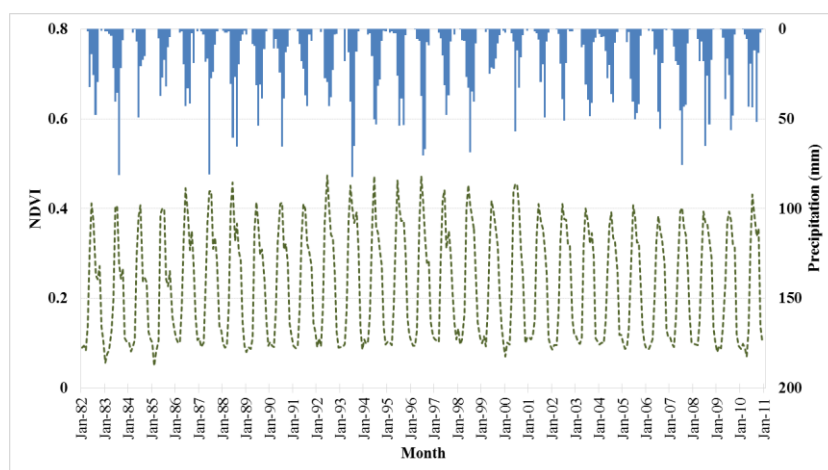


Figure 6. Time series of monthly NDVI (green dashed line) and precipitation (blue bars) for 1982–2010

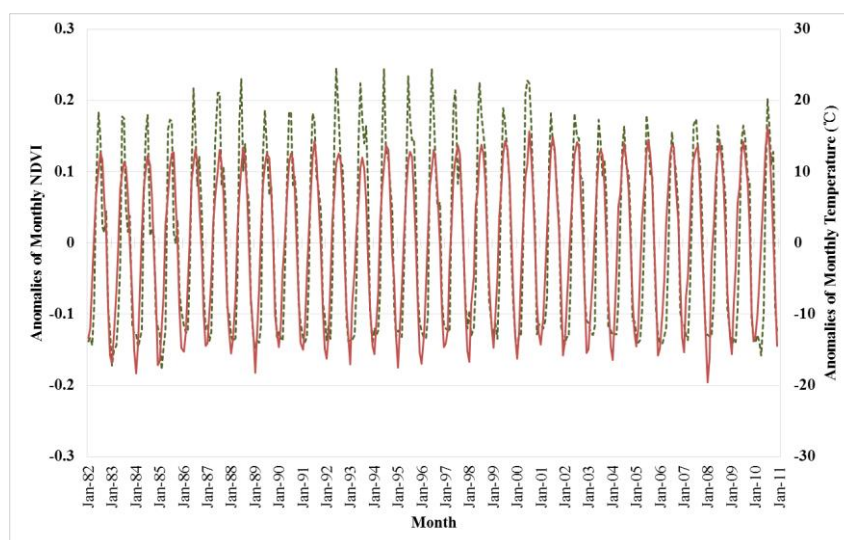


Figure 7. Anomalies of monthly NDVI (green dashed line) and temperature (red line) for 1982–2010

Table 1. Differences in monthly NDVI, mean temperature and precipitation between the beginning of spring (April) and the beginning of summer (June), and between the end of summer (August) and the beginning of winter (November)

Periods	NDVI differences	Temperature differences (°C)	Precipitation differences (mm)
The beginning of spring (April) to the beginning of summer (June)	0.26	16.5	30
The end of summer (August) to the beginning of winter (November)	-0.20	-20.0	-39

Influence of future climate change on vegetation greenness

The monthly observed and simulated NDVI values from 1982 to 2010 are shown in *Figure 8*. Simulations reproduced the timing and range of variation in NDVI reasonably well. The scatter plot of observed to simulated NDVI values demonstrated a strong correlation from the low to high ranges of NDVI (*Fig. 9*). Although R^2 and *MAD* values were lower for model validation than for model training period (*Table 2*), model performance was high enough for both to justify the use of the model for prediction.

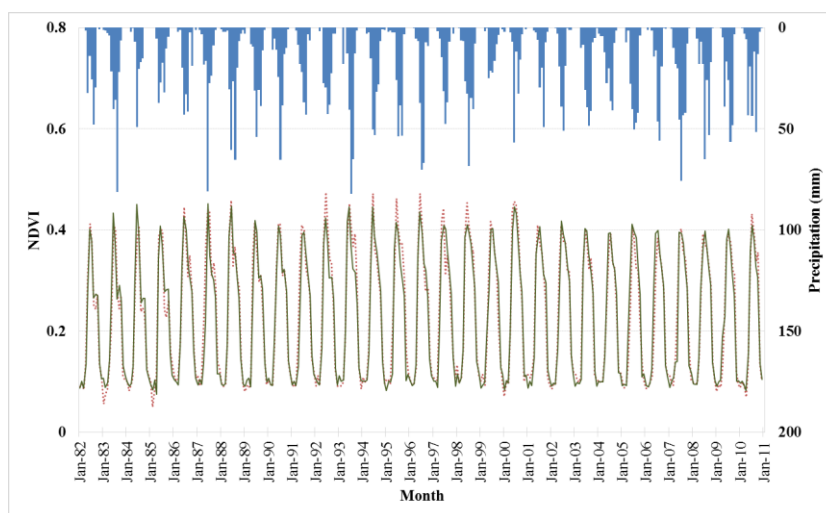


Figure 8. NDVI simulations from 1982 to 2010 in the study area (precipitation: blue bars; observed NDVI: red dashed line; simulated NDVI: green line)

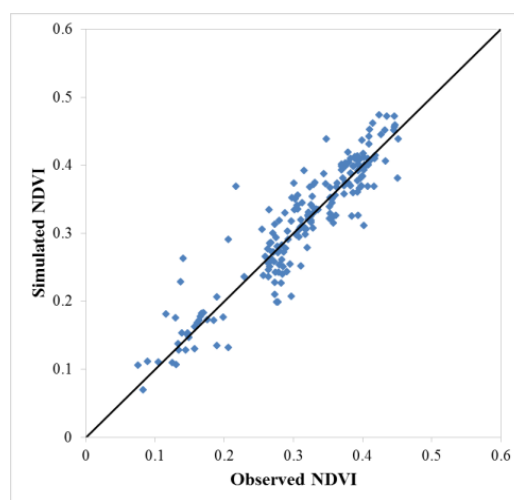


Figure 9. Scatter plot of observed vs. simulated monthly NDVI

Table 2. Model performance for training and validation periods

Performance indicators	Training period (even-numbered years for the period of 1982 to 2010)	Validation period (odd-numbered years for the period of 1982 to 2010)
R^2	0.979	0.922
<i>MAD</i>	0.0117	0.0243

Projected monthly meteorological data for the 2050s under the A1B scenario were used as input for the modified SVIS model to simulate future variation in vegetation greenness. *Figures 10 and 11* depict the changes in monthly precipitation and mean temperature in the Heihe River Basin between the baseline and future climate scenario for the 2050s. Simulations predicted increases in mean monthly precipitation in all months except July, with particularly high increases (>30%) from November to March. Monthly mean temperature was predicted to increase in all months in the 2050s scenario, with an average increase of 2.77 °C. Both precipitation and rainfall were predicted to increase in spring, summer and winter (*Fig. 12*).

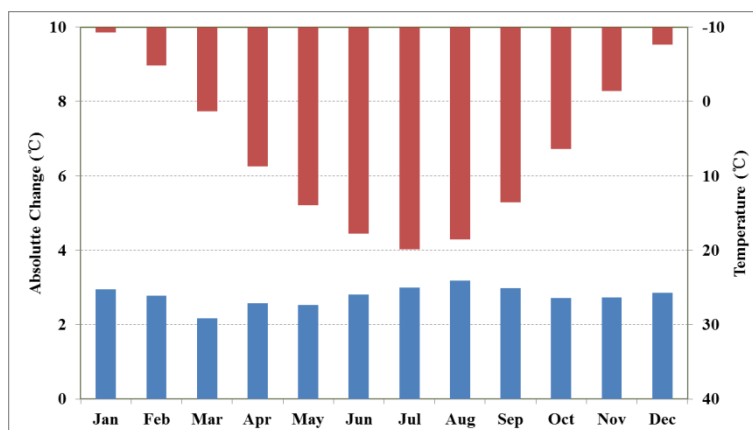


Figure 10. Monthly temperature in the baseline period (red bars) and absolute changes of monthly temperature between baseline period and the projected climate scenario for the 2050s (blue bars)

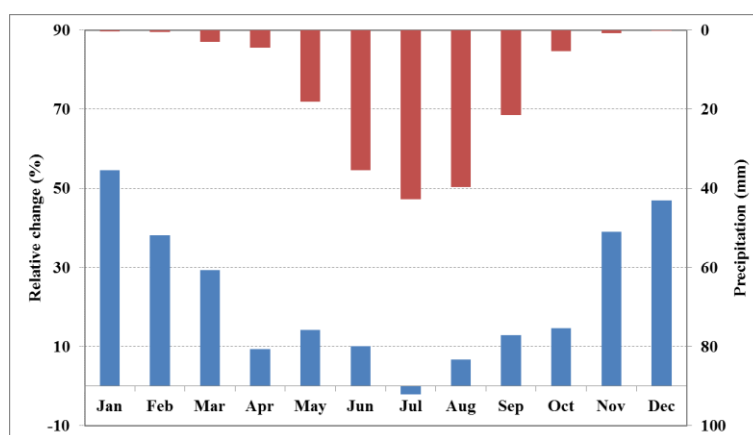


Figure 11. Monthly precipitation in the baseline period (red bars) and absolute changes of monthly precipitation between baseline period and the projected climate scenario for the 2050s (blue bars)

Future climatic scenario and predicted seasonal changes in NDVI are shown in *Figure 12*. Compared with the baseline period, spring and autumn NDVI were predicted to increase 3.8% and 7.9%. Increased precipitation would raise soil water content, benefitting vegetation growth. Carl et al. (2013) demonstrated that global warming may cause temporal shifts in phenology. More specifically, Piao et al. (2008) and Richardson

et al. (2010) indicated that increasing spring and autumn temperature extend the length of growing season and correspondingly the days for biomass growth becomes more available. Yang et al. (2012) indicates that, among different climate factors, temperature and precipitations have closest relations with NDVI. Together, for the study site, increased temperature and precipitation may explain projected increases in NDVI with climate change of spring and autumn. In summer, there is an increase of 3.9% for future NDVI. Both temperature and precipitation rises in summer of the 2050s. Rising temperature would increase the energy available for soil water evaporation and thus reducing the soil water content available for vegetation growth. However, the reduction in soil moisture may be compensated by the increases in precipitation and these increases even finally lead to a rising in soil moisture, which may be the reason that NDVI become higher in summer of the 2050s.

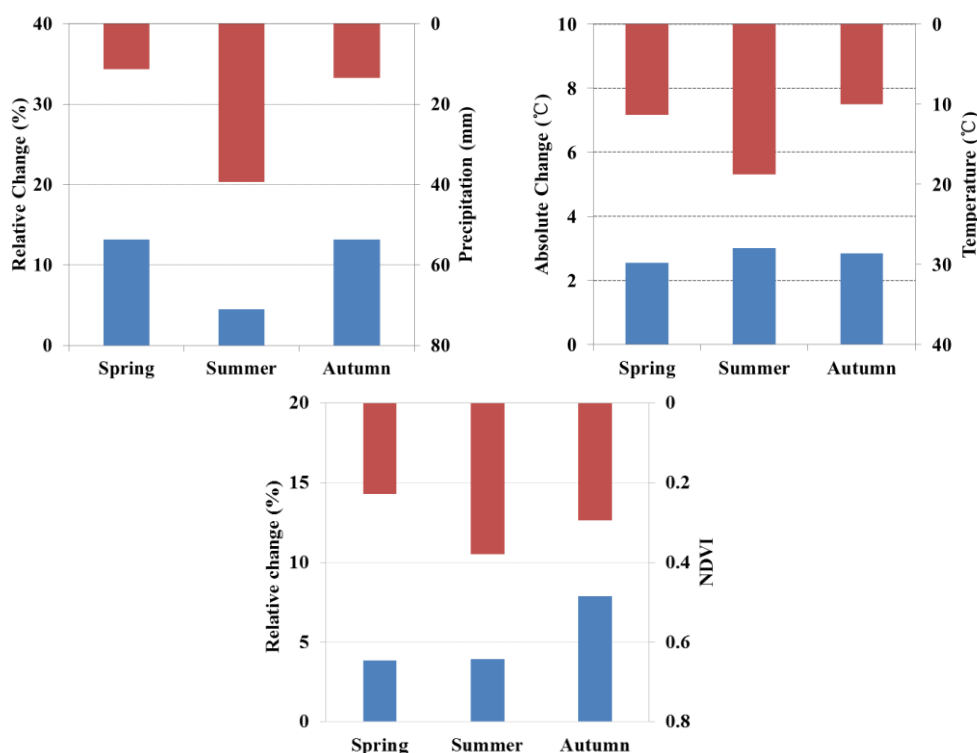


Figure 12. Average changes (blue bars) in seasonal mean precipitation, temperature and simulated NDVI between baseline (red bars) and the projected climate scenario for the 2050s

Our prediction shows that for this dominant shrub in the study area, i.e. *Salsola passerina*, the vegetation greenness become better with the increases in temperature and precipitation. By using a dynamic global vegetation model forced with future climate change scenario, similar results are obtained by Gao et al. (2016) in the Qinghai-Tibetan Plateau, which is adjacent to the Heihe River Basin. Different results are revealed in the study of Gremer et al. (2015), which found that C4 grassland cover negatively responded to mean annual precipitation in the dryland across the south western United States. It is indicated that how natural vegetation responses to climate changes also depends on vegetation type and geophysical conditions. Similarly, Zhang et al. (2016) demonstrated that different vegetation types had very different sensitivities to climate factors in arid Central Asia. The results from model simulation in this study show that

the increased vegetation greenness is caused by the increases of temperature and precipitation. Tang et al. (2017) demonstrated that the sensitivity of vegetation growth to the temperature and precipitation may decrease if these two climatic variables keep increasing in the Shiyang River Basin, which is also located in Northwest China and close to the Heihe River Basin. To further improve our understanding about influences of climate change on natural vegetation in dryland, regional studies based on long-term physiological and phenological observations are necessary.

Conclusions

This study focused on predicting the climate change response of *Salsola passerina*, a representative vegetation type in the middle Heihe Basin, China, using a modified SVIS model. The relationship between satellite-observed NDVI, an indicator of vegetation greenness, and meteorological forcing (temperature and precipitation) were evaluated with the model using 29-year datasets. The performance of both model training and validation justified use of the model for prediction. Climate change scenario data for the 2050s were constructed using the ensemble average of downscaled output from sixteen GCMs for a medium CO₂ emission scenario (A1B). NDVI was projected to increase 3.8% and 7.9% in the spring and autumn, likely because of greater soil water content with increasing precipitation and extension of growing season due to higher temperatures. Projected NDVI rises about 3.9% in the summer seasons, suggesting that increase of soil moisture due to greater precipitation is superior to loss of soil moisture caused by higher temperature. This study focused on the influence of climate change on the growth of *Salsola passerina*. Further understanding of how natural vegetation in the middle Heihe River Basin will react to a changing environment requires the direct incorporation of soil moisture into the SVIS model. Reliable estimation of soil moisture in this region needs a coupled model of both surface water and groundwater to account for human activity such as the use of river water and pumped groundwater for irrigation.

Acknowledgements. This study was supported by the National Key Research and Development Program of China (Grant Nos. 2018YFC0406502, 2016YFC0401308), and the National Natural Science Foundation of China (Grant No. 41671018).

REFERENCES

- [1] Alo, C. A., Wang, G. (2008): Hydrological impact of the potential future vegetation response to climate changes projected by 8 GCMs. – *Journal of Geophysical Research Biogeosciences* 113(G3): 137-149.
- [2] Carl, G., Doktor, D., Koslowsky, D., Kühn, I. (2013): Phase difference analysis of temperature and vegetation phenology for beech forest: a wavelet approach. – *Stochastic Environmental Research and Risk Assessment* 27(5): 1221-1230.
- [3] Fensholt, R., Sandholt, I., Rasmussen, M. S. (2004): Evaluation of MODIS LAI, fAPAR and the relation between fAPAR and NDVI in a semi-arid environment using in situ measurements. – *Remote Sensing of Environment* 91(3-4): 490-507.
- [4] Fensholt, R., Langanke, T., Rasmussen, K., Reenberg, A., Prince, S. D., Tucker, C., Scholes, R. J., Le, Q. B., Bondeau, A., Eastman, R., Epstein, H., Gaughan, A. E., Hellden, A., Mbow, C., Olsson, L., Paruelo, J., Schweitzer, C., Seaquist, J., Wessels, K. (2012): Greenness in semi-arid areas across the globe 1981–2007—an Earth Observing

- Satellite based analysis of trends and drivers. – *Remote Sensing of Environment* 121: 144-158.
- [5] Gao, Q., Guo, Y., Xu, H., Ganjurjav, H., Li, Y., Wan, Y., Qin, X., Ma, X., Liu, S. (2016): Climate change and its impacts on vegetation distribution and net primary productivity of the alpine ecosystem in the Qinghai-Tibetan Plateau. – *Science of the Total Environment* 554-555: 34-41.
- [6] Gessner, U., Naeimi, V., Klein, I., Kuenzer, C., Klein, D., Dech, S. (2013): The relationship between precipitation anomalies and satellite-derived vegetation activity in Central Asia. – *Global and Planetary Change* 110: 74-87.
- [7] Gremer, J. R., Bradford, J. B., Munson, S. M., Duniway, M. C. (2015): Desert grassland responses to climate and soil moisture suggest divergent vulnerabilities across the southwestern United States. – *Global Change Biology* 21(11): 4049-4062.
- [8] Huang, C., Zheng, X., Tait, A., Dai, Y., Yang, C., Chen, Z., Li, T., Wang, Z. (2014): On using smoothing spline and residual correction to fuse rain gauge observations and remote sensing data. – *Journal of Hydrology* 508: 410-417.
- [9] Krishnaswamy, J., John, R., Joseph, S. (2014): Consistent response of vegetation dynamics to recent climate change in tropical mountain regions. – *Global Change Biology* 20(1): 203-215.
- [10] Lal, R. (2004): Carbon sequestration in dryland ecosystems. – *Environmental Management* 33(4): 528-544.
- [11] Li, T., Zheng, X., Dai, Y., Yang, C., Chen, Z., Zhang, S., Wu, G., Wang, Z., Huang, C., Shen, Y., Liao, R. (2014): Mapping near-surface air temperature, pressure, relative humidity and wind speed over mainland China with high spatiotemporal resolution. – *Advances in Atmospheric Sciences* 31(5): 1127-1135.
- [12] Li, Z., Huffman, T., McConkey, B., Townley-Smith, L. (2013): Monitoring and modeling spatial and temporal patterns of grassland dynamics using time-series MODIS NDVI with climate and stocking data. – *Remote Sensing of Environment* 138: 232-244.
- [13] Li, Z., Chen, Y., Li, W., Deng, H., Fang, G. (2015): Potential impacts of climate change on vegetation dynamics in Central Asia. – *Journal of Geophysical Research: Atmospheres* 120(24): 12345-12356.
- [14] Liu, Q., Fu, Y., Zeng, Z., Huang, M., Li, X., Piao, S. (2016): Temperature, precipitation, and insolation effects on autumn vegetation phenology in temperate China. – *Global Change Biology* 22(2): 644-655.
- [15] Los, S. O., Weedon, G. P., North, P. R. J., Kaduk, J. D., Taylor, C. M., Cox, P. M. (2006): An observation-based estimate of the strength of rainfall-vegetation interactions in the Sahel. – *Geophysical Research Letters* 33(16): L16402.
- [16] Lu, L., Li, X., Cheng, G. (2003): Landscape evolution in the middle Heihe River Basin of north-west China during the last decade. – *Journal of Arid Environments* 53(3): 395-408.
- [17] MEA (2005): *Ecosystems and Human Well-Being: Desertification Synthesis*. – Millennium Ecosystem Assessment.
- [18] Ott, K., Kerschbaumer, L., Köbbing, J., Thevs, N. (2016): Bringing sustainability down to earth: Heihe River as a paradigm case of sustainable water allocation. – *Journal of Agricultural and Environmental Ethics* 29(5): 835-856.
- [19] Palmer, R. N., Clancy, E., VanRheenen, N. T., Wiley, M. W. (2004): The impacts of climate change on the Tualatin River Basin water supply: an investigation into projected hydrologic and management impacts. – Prepared for Clean Water Services. DOI: 10.7915/CIG73T9FD.
- [20] Piao, S., Fang, J., Zhou, L., Ciais, P., Zhu, B. (2006): Variations in satellite-derived phenology in China's temperate vegetation. – *Global Change Biology* 12(4): 672-685.
- [21] Piao, S., Ciais, P., Friedlingstein, P., Peylin, P., Reichstein, M., Luysaert, S., Margolis, H., Fang, J., Barr, A., Chen, A., Grelle, A., Hollinger, D. Y., Laurila, T., Lindroth, A., Richardson, A. D., Vesala, T. (2008): Net carbon dioxide losses of northern ecosystems in response to autumn warming. – *Nature* 451(7174): 49.

- [22] Piao, S., Wang, X., Ciais, P., Zhu, B., Wang, T., Liu, J. (2011): Changes in satellite-derived vegetation growth trend in temperate and boreal Eurasia from 1982 to 2006. – *Global Change Biology* 17(10): 3228-3239.
- [23] Pouliot, D., Latifovic, R., Olthof, I. (2009): Trends in vegetation NDVI from 1 km AVHRR data over Canada for the period 1985-2006. – *International Journal of Remote Sensing* 30(1): 20.
- [24] Qi, S., Luo, F. (2007): Environmental degradation problems in the Heihe River Basin, Northwest China. – *Water and Environment Journal* 21(2): 142-148.
- [25] Richardson, A. D., Andy, B. T., Ciais, P., Delbart, N., Friedl, M. A., Gobron, N., Hollinger, D. Y., Kutsch, W. L., Longdoz, B., Luysaert, S., Migliavacca, M., Montagnani, L., Munger, J. W., Moors, E., Piao, S., Rebmann, C., Reichstein, M., Saigusa, N., Tomelleri, E., Vargas, R., Varlagin, A. (2010): Influence of spring and autumn phenological transitions on forest ecosystem productivity. – *Philosophical Transactions of the Royal Society B* 365(1555): 3227-3246.
- [26] Slaymaker, O. (1998): *Physical Geography and Global Environmental Change*. – Longman, Harlow, Essex.
- [27] Smith, B., Samuelsson, P., Wramneby, A., Rummukainen, M. (2011): A model of the coupled dynamics of climate, vegetation and terrestrial ecosystem biogeochemistry for regional applications. – *Tellus A: Dynamic Meteorology and Oceanography* 63(1): 87-106.
- [28] Stellmes, M., Udelhoven, T., Röder, A., Sonnenschein, R., Hill, J. (2010): Dryland observation at local and regional scale. Comparison of Landsat TM/ETM+ and NOAA AVHRR time series. – *Remote Sensing of Environment* 114(10): 2111-2125.
- [29] Sun, W., Song, H., Yao, X., Ishidaira, H., Xu, Z. (2015): Changes in remotely sensed vegetation growth trend in the Heihe Basin of arid northwestern China. – *Plos One* 10(8): e0135376.
- [30] Tang, Z., Ma, J., Peng, H., Wang, S., Wei, J. (2017): Spatiotemporal changes of vegetation and their responses to temperature and precipitation in upper Shiyang River Basin. – *Advances in Space Research* 60(5): 969-979.
- [31] Tschamntke, T., Clough, Y., Wanger, T. C., Jackson, L., Motzke, I., Perfecto, I., Vandermeer, J., Whitbread, A. (2012): Global food security, biodiversity conservation and the future of agricultural intensification. – *Biological Conservation* 151(1): 53-59.
- [32] United Nations Environment Programme (1992): Status of desertification and implementation of the United Nations plan of action to combat desertification. – UNEP Governing Council, 3rd Special Session, Nairobi, KE, 3-5 February 1992.
- [33] Waha, K., Muller, C., Rolinski, S. (2013): Separate and combined effects of temperature and precipitation change on maize yields in sub-Saharan Africa for mid- to late-21st century. – *Global and Planetary Change* 106(C): 1-12.
- [34] Wang, L., D'Odorico, P., Evans, J. P., Eldridge, D. J., McCabe, M. F., Caylor, K., King, E. G. (2012): Dryland ecohydrology and climate change: critical issues and technical advances. – *Hydrology and Earth System Sciences* 16(8): 2585-2603.
- [35] Weston, P., Hong, R., Kaboré, C., Kull, C. (2015): Farmer-managed natural regeneration enhances rural livelihoods in dryland West Africa. – *Environmental Management* 55(6): 1402-1417.
- [36] Wu, D., Wu, H., Zhao, X., Zhou, T., Tang, B., Zhao, W., Jia, K. (2014): Evaluation of spatiotemporal variations of global fractional vegetation cover based on GIMMS NDVI Data from 1982 to 2011. – *Remote Sensing* 6(5): 4217-4239.
- [37] Yang, Y., Xu, J., Hong, Y., Lv, G. (2012): The dynamic of vegetation coverage and its response to climate factors in Inner Mongolia, China. – *Stochastic Environmental Research and Risk Assessment* 26(3): 357-373.
- [38] Zethof, J. H. T., Cammeraat, E. L. H., Nadal-Romero, E. (2019): The enhancing effect of afforestation over secondary succession on soil quality under semiarid climate conditions. – *Science of the Total Environment* 652: 1090-1101.

- [39] Zhang, C., Lu, D., Chen, X., Zhang, Y., Maisupova, B., Tao, Y. (2016): The spatiotemporal patterns of vegetation coverage and biomass of the temperate deserts in Central Asia and their relationships with climate controls. – *Remote Sensing of Environment* 175: 271-281.